Sagittal Fluoroscopy for the Assessment of Hindfoot Kinematics

Benjamin D. McHenry[1]
Department of Biomedical Engineering,
Marquette University,
1515 W. Wisconsin Avenue,
Milwaukee, WI 53233
e-mail: ben.mchenry@mu.edu

Emily Exten
Department of Orthopaedics,
Meriter-UnityPoint Health,
6408 Copps Avenue,
Monona, WI 53716
e-mail: elexten@aol.com

Jason T. Long
Department of OT/PT,
Cincinnati Children's Hospital Medical Center,
3430 Burnet Avenue,
Cincinnati, OH 45229;
Department of Orthopaedic Surgery,
Cincinnati Children's Hospital Medical Center,
3430 Burnet Avenue,
Cincinnati, OH 45229
e-mail: jason.long@cchmc.org

Gerald F. Harris
Department of Biomedical Engineering,
Marquette University,
1515 W. Wisconsin Avenue,
Milwaukee, WI 53233
e-mail: gerald.harris@marquette.edu

Current methods of quantifying foot kinematics during gait typically use markers placed externally on bony anatomic locations. These models are unable to analyze talocrural or subtalar motion because the talus lacks palpable landmarks to place external markers. Alternative methods of measuring these clinically relevant joint motions are invasive and have been limited to research purposes only. This study explores the use of fluoroscopy to noninvasively quantify talocrural and subtalar sagittal plane kinematics. A fluoroscopy system (FS) was designed and built to synchronize with an existing motion analysis system (MAS). Simultaneous fluoroscopic, marker motion, and ground reaction force (GRF) data were collected for five subjects to demonstrate system application. A hindfoot sagittal plane model was developed to evaluate talocrural and subtalar joint motion. Maximum talocrural plantar and dorsiflexion angles averaged among all the subjects occur at 12% and 83% of stance, respectively, with a range of motion of 20.1 deg. Maximum talocrural plantar and dorsiflexion angles averaged among all the subjects occur at toe-off and 67% of stance, respectively, with a range of motion of 8.7 deg. Based on the favorable comparison between the current fluoroscopically measured kinematics and previously reported results from alternative methods, it is concluded that fluoroscopic technology is well suited for measuring the sagittal plane hindfoot motion. [DOI: 10.1115/1.4032445]

Keywords: gait, fluoroscopy, talocrural, subtalar, kinematics

1 Introduction

The need for a clinical foot model capable of uncoupling the talocrural and subtalar joints has been documented in the literature [1–3]. Much of the current clinical research in ankle and hindfoot kinematics focuses on treatments for end-stage ankle arthritis. Outcomes are determined in many studies following total ankle arthroplasty and ankle arthrodesis. Brodsky et al. evaluated 46 patients who underwent a fixed bearing total ankle arthroplasty [1]. The authors found decreased hindfoot range of motion in the sagittal and coronal planes during routine postoperative gait analysis. The study emphasizes the importance of understanding hindfoot mechanics distal to the tibiotalar joint. Another study evaluating sagittal plane motion following ankle arthrodesis showed increased motion of the subtalar joint using static X-rays [2]. These studies highlight the importance of understanding individual motions of the talocrural and subtalar joints during gait.

Most kinematic foot models using skin mounted markers for gait analysis measure calcaneal motion relative to the tibia, effectively combining talocrural and subtalar motions as lumped "ankle" motion [4–9]. Any subtalar specific motion is either not reported or attributed to a neighboring intersegmental joint. This is done because talar position cannot be accurately tracked via externally mounted skin markers [9–11]. Nonetheless, a number of studies have used motion capture data to model the ankle complex as both a talocrural joint and a subtalar joint using motion-based optimization methods [11–14]. While these methods are good at modeling computer generated or mechanical linkage created data, they were found to have angular difference errors in excess of 20 deg when applied to cadaver data [10]. For these reasons, externally placed marker data alone have not been effective in modeling the complex components of motion at the talocrural and subtalar joints.

The use of intracortical bone mounted markers (markers affixed to the end of surgically implanted bone pins) is one way to distinguish individual bones of the foot during in vivo motion tasks. Studies using this technique have described talocrural and subtalar motions in the normal adult population during gait [15,16]. While intracortical bone pin methodologies have been applied for research in healthy adults, their invasive nature precludes widespread application in pathology or pediatrics. Dynamic MRI is an additional methodology that has been used to define in vivo talocrural and subtalar kinematics [17]. While valuable, these MRI systems do not allow data collection during natural gait.

Over the last two decades, fluoroscopy has emerged as a means for tracking the position and orientation of the underlying skeletal anatomy of the foot/ankle [18–28]. The first 2D static kinematic model of the foot based on fluoroscopically collected images was done by Komistek et al. in 2000 [20]. The study measured the range of motion in the sagittal plane between two static positions (maximum flexion/extension). The first 3D static kinematic model of the hindfoot using fluoroscopic images was done by de Asla et al. in 2006 [21]. The model used MRI techniques to create a 3D model of the tibia, fibula, talus, and calcaneus. The fluoroscopic images were used to place the 3D models in the same orientations as seen by the fluoroscopic images. The major drawbacks of de Asla's study were the limited scope of gait studied (heel strike, midstance (MSt), and toe-off), and the static nature of the analysis (subjects stopped moving while the fluoroscopic images were acquired).

Other fluoroscopic studies measuring kinematics of the hindfoot are reported using either single plane fluoroscopy with 3D-to-2D model-based registration [22–25] or biplane fluoroscopy with model-based tracking techniques [26–28]. Both of these approaches are methodologically sound, and both require the patient to undergo

[1]Corresponding author.
Manuscript received March 25, 2015; final manuscript received December 29, 2015; published online January 29, 2016. Assoc. Editor: Paul Rullkoetter.

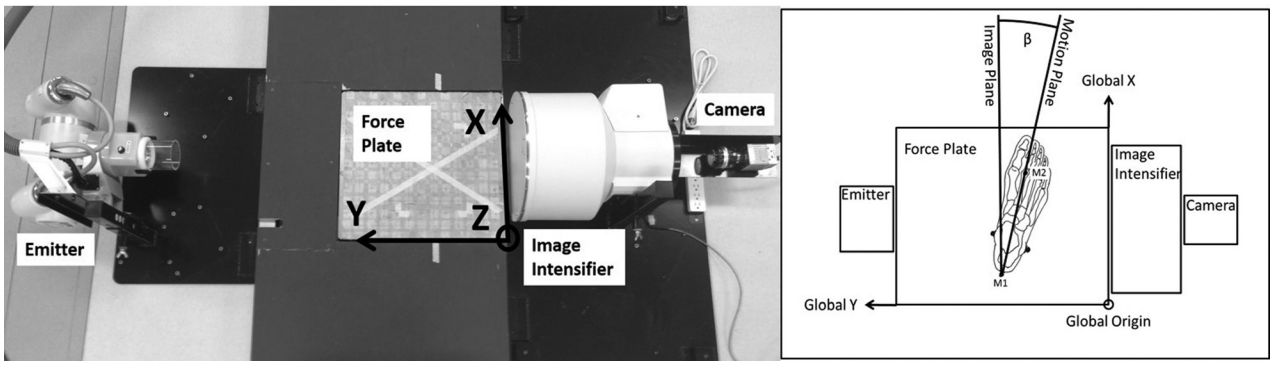

Fig. 1 System configuration (left) showing the embedded force plate with global *X* and *Y* coordinates (*Z* is the cross product of *X* and *Y*), emitter, image intensifier, and the digital camera. Foot position (right) showing the fluoroscopic image plane and sagittal motion plane of the foot which is rotated by foot progression angle (β).

MR or CT imaging in order to generate the 3D bone models. Only one of the aforementioned fluoroscopic studies quantified talocrural and/or subtalar kinematics from the full set of dynamically acquired images on living subjects during gait [28]. Results were reported for a single subject [28].

The goal of the current study was to integrate a single gantry fluoroscope into a motion analysis walkway and to develop the methodology to quantify in vivo sagittal plane talocrural and subtalar kinematics during gait, without the need for CT or MR imaging. System feasibility for clinical application was previously established in a study of 13 young adult participants [3]. The current work presents a technical description of the single gantry FS design, calibration, evaluation, and limitations.

2 Methods

The combined fluoromotion capture system was designed as part of a developed sagittal plane kinematic model of the talocrural and subtlar joints which required synchronous collection of MAS marker, fluoroscopic imaging, and GRF data. The following methodology describes how these data were synchronized as well as the step-by-step process used for the kinematic analysis. Point of interest (POI) locations in the fluoroscopic images were translated to the MAS coordinate system using marker position data and a process called global referencing. Once translated, these POI locations were used along with marker position data to define local coordinate systems for the tibia, talus, and calcaneus in the kinematic model.

The MAS consisted of 14 infrared cameras (Vicon Motion Systems, Inc., Oxford, UK) that tracked standard 16 mm reflective markers. The fluoroscopic images were collected at 120 fps using a Basler Aviator avA1000km camera (Basler Vision Technologies, Ahrensburg, Germany), imaging software called XCAP (EPIX, Inc., Buffalo Grove, IL), and a reconfigured OEC 9000 C-arm fluoroscopy unit (GE, Fairfield, CT). GRF trigger data were collected using a multi-axis AMTI OR6-5-1 force plate (AMTI, Watertown, MA) embedded in a raised walkway. Data processing was done in MATLAB (The MathWorks, Inc., Natick, MA) and ImageJ (NIH). Figure 1 illustrates the FS configuration.

The kinematic analysis required MAS marker data, fluoroscopic POI location data, and GRF magnitudes to be defined in a common coordinate system. The MAS coordinate system was selected because the GRF data were already defined by the MAS. The fluoroscopic images were synchronized to the MAS using a 5 V transistor–transistor logic (TTL) pulse that was generated by the fluoroscopy unit when activated. The pulse was inputted into the Vicon MX motion system as an external device analog signal where it was synchronized with the MAS marker and GRF data. The same TTL pulse was inputted as a general purpose input to the computer with the imaging software, where it was used to trigger the recording of images. Code was written to detect heel strike by quantifying the number of frames between the 5 V TTL trigger (initiating fluoroscopic image recording) and GRF initiation (heel strike). This calculated number corresponded to the number of images collected fluoroscopically before heel strike occurred. High acceleration tests with an impact device were completed to ensure reliable detection of heel strike (± 1 frame at 120 fps).

Pin cushion distortion is a type of radial distortion which can be corrected for by using Brown's distortion model [29], based on earlier work by Conrady [30]. For this study, pin cushion distortion of fluoroscopic images was corrected using a calibration grid and software developed by Karau et al. [31]. After image correction was done, global referencing equations (1)–(3) (Table 1) were applied to translate fluoroscopic POI locations in image coordinates (Fx', Fz') to POI locations in MAS global coordinates (FX, FY, FZ) within the sagittal plane of the foot. These equations account for scaling from pixels to millimeter as well as projecting from the image plane (parallel to the face of the image intensifier) to the sagittal plane of the foot (Fig. 1). All globally referenced POI locations exist within the sagittal plane of the foot which is defined as vertical and containing MAS markers M1 and M2 (see Table 2 for marker locations). The global referencing process requires at least one MAS marker to be in the fluoroscopic field of view (MAS marker M1) and two MAS markers to define foot progression angle β (MAS markers M1 and M2). Image magnification (IM) is determined by dividing the pixel distance between two radiopaque markers attached to the medial shank by the known distance between the two markers (30 mm). Figure 2 shows a typical fluoroscopic image with parameters of Eqs. (1)–(3) identified.

In order to evaluate the use of global referencing equations (1)–(3), experiments were done to quantify the error between globally referenced points in fluoroscopic images and their known global locations in the MAS motion plane. Resolution and accuracy have been established for both adult and pediatric foot MAS capture volumes by our group in prior studies [6,32]. For global referencing evaluation, a matrix of 81 equally spaced radiopaque markers (2 mm diameter) was imaged in several static positions.

Table 1 Equations used for global referencing. Global coordinates (*X*, *Y*, *Z*) in millimeter are anterior, medial, and superior, respectively. Fluoroscopic coordinates (x', z') in pixels are anterior and superior, respectively. IM scales distances in the fluoroscopic images from pixels to millimeter. θ and β are angles measured in degrees.

$F1X = M1X + \left[\left[\frac{F1x'-M1x'}{IM}\right]\cos\theta + \left[\frac{F1z'-M1z'}{IM}\right]\sin\theta\right]$	Eq. (1)
$F1Y = M1Y + \left[\left[\frac{F1x'-M1x'}{IM}\right]\cos\theta + \left[\frac{F1z'-M1z'}{IM}\right]\sin\theta\right]\tan\beta$	Eq. (2)
$F1Z = M1Z + \left[-\left[\frac{F1x'-M1x'}{IM}\right]\sin\theta + \left[\frac{F1z'-M1z'}{IM}\right]\cos\theta\right]$	Eq. (3)

Table 2 External marker locations. Markers M1 and M2 are used to define the foot progression angle (β) in Eq. (2). Markers M3–M6 are used to define the axes of the tibial coordinate system (Table 4).

Marker name	Marker location
M1	Calcaneal tuberosity
M2	Head of the second metatarsal
M3	Medial malleolus
M4	Lateral malleolus
M5	Medial femoral epicondyle
M6	Lateral femoral epicondyle

The markers were located in a 9×9 matrix array (rows and columns spaced at an interval of 25.4 mm). The 2D matrix was rotated in 5 deg increments in the transverse plane and swept through a 90 deg angle (± 45 deg with respect to global X) in order to approximate extreme variations in foot progression angle (β). The radiopaque marker locations were then globally referenced and compared to their known global locations in the MAS. These experiments yielded errors less than 2 mm for points referenced at locations similar to those of the talus and calcaneus with ± 5 deg of foot progression (as was the case for all the five subjects in this study). In addition, these errors were predictable based on position in the capture volume and foot progression angle. This predictability allows for correction algorithms to account for progression angles that exceed ± 5 deg.

The developed hindfoot model analyzes talocrural and subtalar joint kinematics and therefore requires coordinate systems to be defined for the tibia, talus, and calcaneus. The tibia coordinate system was defined by MAS markers M3–M6 (Table 2), as it remained outside the image intensifier field of view for early and late phases of stance. The talus and calcaneus coordinate systems were defined by fluoroscopic markers. Fluoroscopic markers are POI locations on fluoroscopic images that have been translated from image coordinates to global coordinates using global referencing. Each bone (talus and calcaneus) required two fluoroscopic markers (Fig. 3) to define its coordinate system for each fluoroscopic image. Because there are no standard anatomic tracking locations associated with the calcaneus or talus, fluoroscopic marker locations were chosen based on visibility and distinguishability throughout the entire image sequence. In addition,

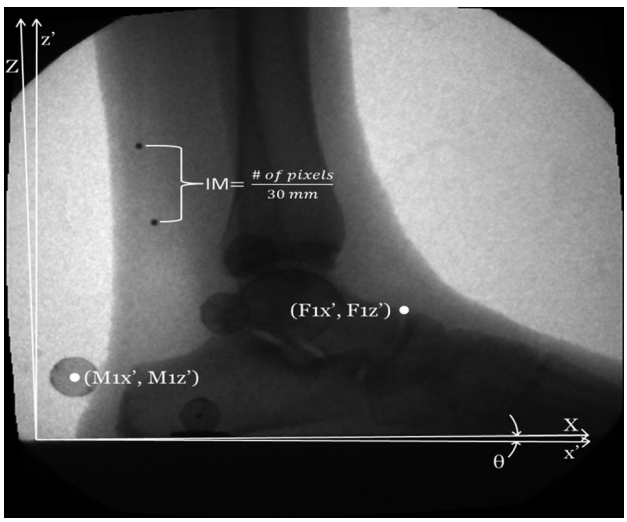

Fig. 2 Typical fluoroscopic image. POI locations are translated from image coordinates (*F1x'*, *F1z'*) to global coordinates (*F1X*, *F1Y*, *F1Z*) using an external marker image (M1*x'*, M1*z'*) and global (M1*X*, M1*Y*, M1*Z*) coordinate locations, as well as the IM, subject foot progression angle (β, calculated from external markers), and camera static angular rotation from global (θ).

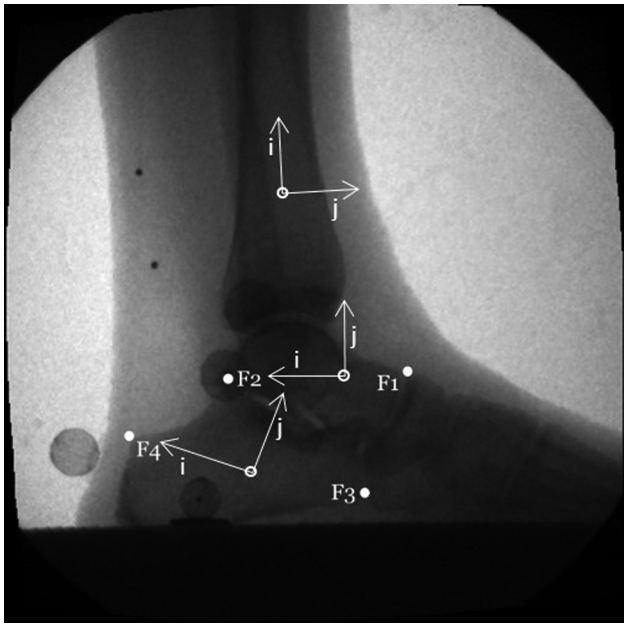

Fig. 3 Fluoroscopic markers and local coordinate axes. F1 and F2 represent the fluoroscopic marker locations for the talus, while F3 and F4 represent the fluoroscopic marker locations for the calcaneus. Local coordinate axes for the tibia, talus, and calcaneus are also shown. Local *k*-axes (not shown) are the cross of local *i*-axes with local *j*-axes.

fluoroscopic marker locations were selected as far apart as possible. For this study, the following fluoroscopic marker locations were used (as shown in Fig. 3): F1—superior border of the talonavicular joint; F2—posterior talar process; F3—inferior aspect of the calcaneocuboid joint; and F4—superior aspect of the posterior tuberosity of the calcaneus. As part of the system evaluation, both intraclinician and interclinician discrepancies in locating the same fluoroscopic markers frame to frame are reported (Table 3).

Once fluoroscopic marker locations were translated to global coordinates, they were used in conjunction with MAS markers (Table 2) to define the coordinate axes of the tibia, talus, and calcaneus coordinate systems (Table 4). Tibial i-axis is a unit vector pointing superiorly from the midpoint between MAS markers M3 and M4 to the midpoint between MAS markers M5 and M6. Tibial j-axis is a unit vector that points anteriorly and is the cross product of a temporary vector (starting from the midpoint between MAS markers M3 and M4 pointing toward MAS marker M3) with the tibial i-axis. The tibial k-axis points medially and is the cross product of the tibial i-axis with the tibial j-axis. Talar i-axis is a unit vector that points from FS marker F1 to FS marker F2. Talar k-axis is a unit vector that points medially and is the cross product of talar i-axis with global Z (0,0,1). Talar j-axis is the cross product of the talar k-axis with the talar i-axis. Calcaneal i-axis is a unit vector that points from FS marker F3 to FS marker F4. Calcaneal k-axis is a unit vector that points medially and is the cross product of calcaneal i-axis with global Z (0,0,1). Calcaneal j-axis is the cross product of the calcaneal k-axis with the calcaneal i-axis.

Table 3 Intraclinician and interclinician discrepancies in locating the same fluoroscopic markers frame to frame

	Intraexaminer		Interexaminer	
	Mean	SD	Mean	SD
Three-dimensional positional differences in fluoroscopic marker locations (mm)	1.41	1.04	1.63	0.95
Kinematic differences based on 3D positional differences (deg)	1.06	0.81	1.44	1.00

Table 4 Segment local coordinate system axes definition. Fluoroscopic markers have prefix *F* and are globally referenced points from the fluoroscopic images (Fig. 3). External markers have prefix *M* and are defined by the MAS. All marker locations are described in global coordinates.

Segment	*i*-axis	*j*-axis	*k*-axis
Calcaneus	$\frac{(F4-F3)}{\lvert(F4-F3)\rvert}$	$\frac{(k_{axis}\times i_{axis})}{\lvert(k_{axis}\times i_{axis})\rvert}$	$\frac{(i_{axis}\times(0,0,1))}{\lvert(i_{axis}\times(0,0,1))\rvert}$
Talus	$\frac{(F2-F1)}{\lvert(F2-F1)\rvert}$	$\frac{(k_{axis}\times i_{axis})}{\lvert(k_{axis}\times i_{axis})\rvert}$	$\frac{(i_{axis}\times(0,0,1))}{\lvert(i_{axis}\times(0,0,1))\rvert}$
Tibia	$\frac{\left(\frac{M5+M6}{2}\right)-\left(\frac{M3+M4}{2}\right)}{\left\lvert\left(\left(\frac{M5+M6}{2}\right)-\left(\frac{M3+M4}{2}\right)\right)\right\rvert}$	$\frac{\left(\left(M3-\left(\frac{M3+M4}{2}\right)\right)\times i_{axis}\right)}{\left\lvert\left(\left(M3-\left(\frac{M3+M4}{2}\right)\right)\times i_{axis}\right)\right\rvert}$	$\frac{(i_{axis}\times j_{axis})}{\lvert(i_{axis}\times j_{axis})\rvert}$

After coordinate definition, kinematic analysis was completed by using the Joint Coordinate Method recommended by the International Society of Biomechanics (ISB) [33,34], with motion being reported as distal segment movement with respect to proximal. Although this is a 2D study, the kinematic model was triaxial. By definition, talar and calcaneal local *k*-axes (Table 4) are parallel to each other and perpendicular to the sagittal (motion) plane. To ensure proper coordinate definition, coronal and transverse plane motions about the subtalar joint are measured to verify a magnitude of zero.

In addition to the dynamic fluoroscopic images, the kinematic model was applied to a static X-ray image with the subject standing in a weight-bearing position. The same fluoroscopic marker locations used in the dynamic kinematic model (Fig. 3) were used in the static model. This static model measured talocrural and subtalar sagittal plane angles during quiet standing. These measured angles represent neutral position (0 deg) for reported kinematics. Defining quiet standing as neutral position allows for the use of subject-specific, and even trial-specific, fluoroscopic marker locations (Fig. 3). It is critical, however, that the same locations be used within a trial.

Five clinically healthy male subjects (22.8 yr [4.0 SD], 1.77 m [0.04 SD], 72.6 kg [4.1 SD]) participated in the study to demonstrate the system/kinematic model. Informed consent was obtained in compliance with the IRB requirements. Each subject completed four barefoot walking trials at a self-selected pace while wearing protective shielding. Effective dose levels were estimated at 10 μSv per trial.

3 Results

Sagittal plane kinematic results for both the talocrural and subtalar joints for a single subject are presented in Fig. 4. All the four trials are plotted and results are subdivided into standardized phases of stance [35]. Sagittal plane kinematic results for both the talocrural and subtalar joints for all the five subjects are presented in Fig. 5. Mean and standard deviation of all subjects' trials (5 subjects, 4 trials per subject, 20 trials total) are subdivided into standardized phases of stance [35]. The missing data at the end of preswing (PSw) corresponds to the foot vacating the field of view. Figures 4 and 5 show the talocrural joint increasing to maximum plantar flexion during loading response followed by dorsiflexion motion during MSt and terminal stance (TSt). Maximum talocrural dorsiflexion occurs at the beginning of PSw followed by plantarflexion toward swing phase. Figures 4 and 5 show the subtalar joint in a neutral position at heel strike followed by dorsiflexion into MSt. Maximum subtalar dorsiflexion occurs during TSt at which point plantar flexion occurs for the rest of stance.

4 Discussion

It is generally accepted that the talus cannot be accurately tracked by the markers attached to the surface of the skin [9–11]. While a number of studies have used motion capture data of the shank and foot to model the ankle complex as both a talocrural joint and a subtalar joint using motion-based optimization methods [11–14], accuracy results suggest that in vivo application may be limited [10]. Because of this, most current kinematic MAS models report only ankle joint motion, or that of a hindfoot/calcaneal segment with respect to a shank segment [4–9]. The ankle joint kinematic results from these models compare favorably to the talocrural results of the current study both in morphology and range of motion.

Bone pin methodologies do allow discrete talar isolation and are capable of reporting talocrural and subtalar motion in vivo. Results from these bone pin studies compare favorably to that of this work. Sagittal plane talocrural joint kinematic graphs from two bone pin studies ($n = 8$) show maximum plantar flexion occurring before 15% of stance and maximum dorsiflexion (with the exception of one subject) occurring after 75% of stance with range of motion values between 11.3 deg and 18.7 deg [15,16]. The fluoroscopic maximum talocrural plantar and dorsiflexion angles averaged among all subjects occur at 12% and 83% of stance, respectively (Fig. 5), with a range of motion of 20.1 deg. Sagittal plane subtalar joint kinematic graphs from the same bone pin studies show varied locations of maximum plantar and dorsiflexion and ranges of motion between 2.8 deg and 8.8 deg. The fluoroscopic maximum talocrural plantar and dorsiflexion angles averaged among all subjects occur at toe-off (97%) and 67% of stance, respectively (Fig. 5), with a range of motion of 8.7 deg. The invasive nature, risk of infection, and gait altering potential associated with bone pin insertion limit widespread clinical application. These methodological constraints do not exist with the fluoroscopic model, potentially making its application to pathology and pediatrics more palatable to clinicians and parents.

A recent biplane fluoroscopic study quantified talocrural and subtalar kinematics during gait of a single subject from a set of dynamically acquired images [28]. Sagittal plane kinematic

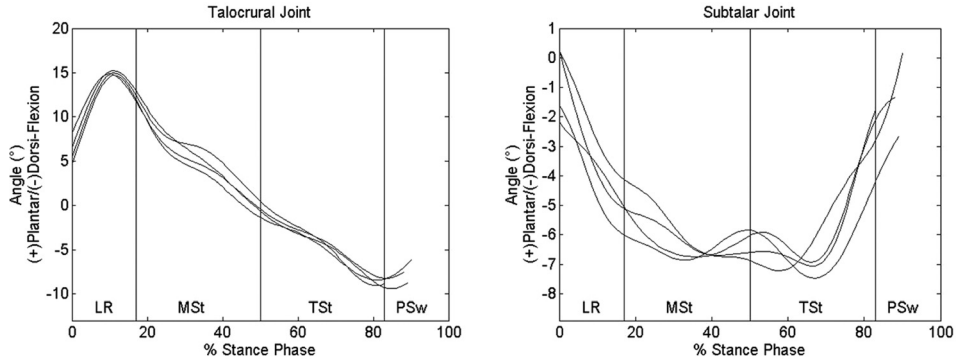

Fig. 4 Talocrural (left) and subtalar (right) plantar/dorsiflexion angles (single subject, four trials)

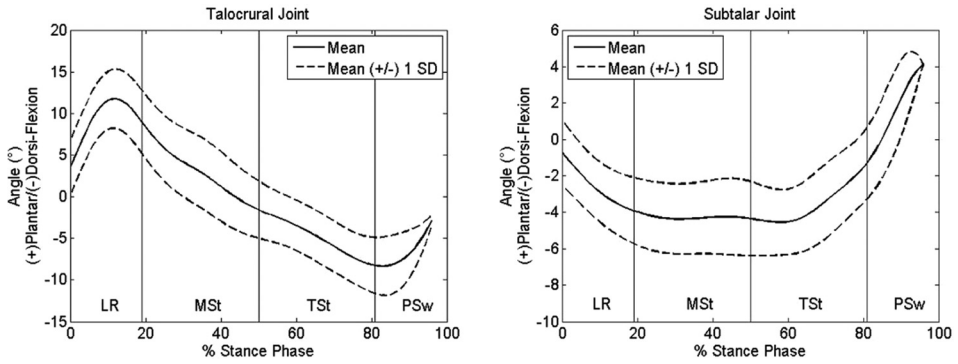

Fig. 5 Talocrural (left) and subtalar (right) plantar/dorsiflexion angles (five subjects, four trials per subject)

results from the currently reported single gantry system compare favorably to the biplane study. Because the biplane methodology split stance phase into two different data collection trials (heel strike and toe-off), a piecewise comparison was done. The morphology of graphs between the studies shows comparable results at heel strike, early MSt, and late MSt. The biplane study reported a total estimated dose equivalent of less than 120 μSv, which included a foot/ankle CT at 1 mm slice thicknesses. The single gantry system does not require a CT, and for four walking trials, the total estimated dose equivalent is conservatively estimated at no greater than 50 μSv, which includes a static weight-bearing lateral X-ray of the foot/ankle.

While the current 2D FS demonstrates the feasibility of using fluoroscopic technology to track intrafoot motion, there are limitations. In clinical applications where in vivo sagittal plane kinematics are of interest, the 2D system is appropriate. In applications where information is needed on coronal and/or transverse motion, a biplane system is recommended. For the current study, the selected camera speed of 120 fps was sufficient for walking trials, but may need to be increased for higher speed activities, such as running. An additional study should be completed to ensure that ambulation in footwear, such as shoes, orthotics, and braces, can be captured with the same image quality. The study limitations include the 2D nature of the analysis. While a second FS would allow a full 3D analysis, the single gantry system has shown ability in quantifying sagittal plane talocrural and subtalar kinematics with less than half the radiation of a biplane system, depending on the imaging technique used for model-based tracking (CT or MRI). An additional limitation is the use of ionizing radiation. Levels of the currently reported system were estimated at 10 μSv per trial. This is far below the USNRC whole body annual occupational limit of 5 rems (50,000 μSv) [36].

5 Conclusion

The purpose of this study was to develop the unique hardware and methodology to use single plane fluoroscopy to quantify in vivo sagittal plane talocrural and subtalar kinematics during gait, without the need for CT or MR imaging. The dynamic radiographic nature of fluoroscopy lends itself toward quantifying the in vivo bony motion of the foot. It is concluded on the basis of the current study that controlled fluoroscopy within a motion analysis environment is appropriate for assessment of sagittal plane talocrural and subtalar kinematics. The hindfoot motion reported in this study compares favorably to standard MAS models only capable of measuring calcaneal to tibia motion, biplane fluoroscopic models using model-based tracking, and invasive bone pin talocrural and subtalar results.

Acknowledgment

The contents of this study were developed under grants from the Department of Education, NIDRR Grant Nos. H133E100007 and H133P080005. However, the contents do not necessarily represent the policy of the Department of Education, and you should not assume endorsement by the Federal Government. This study was additionally supported by Shriners Hospitals for Children and the Pedorthic Foundation.

References

[1] Brodsky, J. W., Coleman, S. C., Smith, S., Polo, F. E., and Tenenbaum, S., 2013, "Hindfoot Motion Following STAR Total Ankle Arthroplasty A Multi-segment Foot Model Gait Study," Foot Ankle Int., **34**(11), pp. 1479–1485.
[2] Sealey, R. J., Myerson, M. S., Molloy, A., Gamba, C., Jeng, C., and Kalesan, B., 2009, "Roger Mann Award 2008: Sagittal Plane Motion of the Hindfoot Following Ankle Arthrodesis: A Prospective Analysis," Foot Ankle Int., **30**(3), pp. 187–196.
[3] McHenry, B. D., Exten, E. L., Long, J., Law, B., Marks, R. M., and Harris, G., 2014, "Sagittal Subtalar and Talocrural Joint Assessment With Weight-Bearing Fluoroscopy During Barefoot Ambulation," Foot Ankle Int., pp. 430–435.
[4] Carson, M. C., Harrington, M. E., Thompson, N., O'Connor, J. J., and Theologis, T. N., 2001, "Kinematic Analysis of a Multi-Segment Foot Model for Research and Clinical Applications: A Repeatability Analysis," J. Biomech., **34**(10), pp. 1299–1307.
[5] Hunt, A. E., Smith, R. M., Torode, M., and Keenan, A. M., 2001, "Inter-Segment Foot Motion and Ground Reaction Forces Over the Stance Phase of Walking," Clin. Biomech. (Bristol, Avon), **16**(7), pp. 592–600.
[6] Kidder, S. M., Abuzzahab, F. S., Jr., Harris, G. F., and Johnson, J. E., 1996, "A System for the Analysis of Foot and Ankle Kinematics During Gait," IEEE Trans. Rehabil. Eng., **4**(1), pp. 25–32.
[7] Leardini, A., Benedetti, M. G., Berti, L., Bettinelli, D., Nativo, R., and Giannini, S., 2007, "Rear-Foot, Mid-Foot and Fore-Foot Motion During the Stance Phase of Gait," Gait Posture, **25**(3), pp. 453–462.
[8] Leardini, A., Benedetti, M. G., Catani, F., Simoncini, L., and Giannini, S., 1999, "An Anatomically Based Protocol for the Description of Foot Segment Kinematics During Gait," Clin. Biomech. (Bristol, Avon), **14**(8), pp. 528–536.
[9] MacWilliams, B. A., Cowley, M., and Nicholson, D. E., 2003, "Foot Kinematics and Kinetics During Adolescent Gait," Gait Posture, **17**(3), pp. 214–224.
[10] Lewis, G. S., Sommer, H., and Piazza, S. J., 2006, "In Vitro Assessment of a Motion-Based Optimization Method for Locating the Talocrural and Subtalar Joint Axes," ASME J. Biomech. Eng., **128**(4), pp. 596–603.
[11] van den Bogert, A. J., Smith, G. D., and Nigg, B. M., 1994, "In Vivo Determination of the Anatomical Axes of the Ankle Joint Complex: An Optimization Approach," J. Biomech., **27**(12), pp. 1477–1488.
[12] Pierrynowski, M. R., Finstad, E., Kemecsey, M., and Simpson, J., 2003, "Relationship Between the Subtalar Joint Inclination Angle and the Location of Lower-Extremity Injuries," J. Am. Podiatr. Med. Assoc., **93**(6), pp. 481–484.
[13] Reinbolt, J. A., Schutte, J. F., Fregly, B. J., Koh, B. I., Haftka, R. T., George, A. D., and Mitchell, K. H., 2005, "Determination of Patient-Specific Multi-Joint Kinematic Models Through Two-Level Optimization," J. Biomech., **38**(3), pp. 621–626.
[14] Siston, R. A., Daub, A. C., Giori, N. J., Goodman, S. B., and Delp, S. L., 2005, "Evaluation of Methods That Locate the Center of the Ankle for Computer-Assisted Total Knee Arthroplasty," Clin. Orthop. Relat. Res., **439**, pp. 129–135.
[15] Arndt, A., Westblad, P., Winson, I., Hashimoto, T., and Lundberg, A., 2004, "Ankle and Subtalar Kinematics Measured With Intracortical Pins During the Stance Phase of Walking," Foot Ankle Int., **25**(5), pp. 357–364.
[16] Lundgren, P., Nester, C., Liu, A., Arndt, A., Jones, R., Stacoff, A., Wolf, P., and Lundberg, A., 2008, "Invasive In Vivo Measurement of Rear-, Mid- and Forefoot Motion During Walking," Gait Posture, **28**(1), pp. 93–100.
[17] Sheehan, F. T., Seisler, A. R., and Siegel, K. L., 2007, "In Vivo Talocrural and Subtalar Kinematics: A Non-Invasive 3D Dynamic MRI Study," Foot Ankle Int., **28**(3), pp. 323–335.
[18] Perlman, P. R., Dubois, P., and Siskind, V., 1996, "Validating the Process of Taking Lateral Foot X-Rays," J. Am. Podiatr. Med. Assoc., **86**(7), pp. 317–321.

[19] Wearing, S. C., Smeathers, J. E., Yates, B., Sullivan, P. M., Urry, S. R., and Dubois, P., 2005, "Errors in Measuring Sagittal Arch Kinematics of the Human Foot With Digital Fluoroscopy," Gait Posture, **21**(3), pp. 326–332.
[20] Komistek, R. D., Stiehl, J. B., Buechel, F. F., Northcut, E. J., and Hajner, M. E., 2000, "A Determination of Ankle Kinematics Using Fluoroscopy," Foot Ankle Int., **21**(4), pp. 343–350.
[21] de Asla, R. J., Wanm, L., Rubash, H. E., and Li, G., 2006, "Six DOF In Vivo Kinematics of the Ankle Joint Complex: Application of a Combined Dual-Orthogonal Fluoroscopic and Magnetic Resonance Imaging Technique," J. Orthop. Res., **24**(5), pp. 1019–1027.
[22] Fukano, M., and Fukubayashi, T., 2014, "Changes in Talocrural and Subtalar Joint Kinematics of Barefoot Versus Shod Forefoot Landing," J. Foot Ankle Res., **7**(1), p. 42.
[23] Kobayashi, T., No, Y., Yoneta, K., Sadakiyo, M., and Gamada, K., 2013, "In Vivo Kinematics of the Talocrural and Subtalar Joints With Functional Ankle Instability During Weight-Bearing Ankle Internal Rotation: A Pilot Study," Foot Ankle Spec., **6**(3), pp. 178–184.
[24] Kobayashi, T., Saka, M., Suzuki, E., Yamazaki, N., Suzukawa, M., Akaike, A., Shimizu, K., and Gamada, K., 2014, "In Vivo Kinematics of the Talocrural and Subtalar Joints During Weightbearing Ankle Rotation in Chronic Ankle Instability," Foot Ankle Spec., **7**(1), pp. 13–19.
[25] Yamaguchi, S., Sasho, T., Kato, H., Kuroyanagi, Y., and Banks, S. A., 2009, "Ankle and Subtalar Kinematics During Dorsiflexion-Plantarflexion Activities," Foot Ankle Int., **30**(4), pp. 361–366.
[26] Kozanek, M., Rubash, H. E., Li, G., and Richard, J., 2009, "Effect of Post-Traumatic Tibiotalar Osteoarthritis on Kinematics of the Ankle Joint Complex," Foot Ankle Int., **30**(8), pp. 734–740.
[27] Campbell, K. J., Wilson, K. J., LaPrade, R. F., and Clanton, T. O., 2014, "Normative Rearfoot Motion During Barefoot and Shod Walking Using Biplane Fluoroscopy," Knee Surg., Sports Traumatol., Arthrosc., epub.
[28] Wang, B., Roach, K. E., Kapron, A. L., Fiorentino, N. M., Saltzman, C. L., Singer, M., and Anderson, A. E., 2015, "Accuracy and Feasibility of High-Speed Dual Fluoroscopy and Model-Based Tracking to Measure In Vivo Ankle Arthrokinematics," Gait Posture, **41**(4), pp. 888–893.
[29] Brown, D. C., 1966, "Decentering Distortion of Lenses," Photometr. Eng., **32**(3), pp. 444–462.
[30] Conrady, A. E., 1919, "Decentred Lens-Systems," Mon. Not. R. Astron. Soc., **79**(5), pp. 384–390.
[31] Karau, K. L., Johnson, R. H., Molthen, R. C., Dhyani, A. H., Haworth, S. T., Hanger, C. C., Roerig, D. L., and Dawson, C. A., 2001, "Microfocal X-Ray CT Imaging and Pulmonary Arterial Distensibility in Excised Rat Lungs," Am. J. Physiol. Heart Circ. Physiol., **281**(3), pp. H1447–H1457.
[32] Myers, K. A., Wang, M., Marks, R. M., and Harris, G. F., 2004, "Validation of a Multisegment Foot and Ankle Kinematic Model for Pediatric Gait," IEEE Trans. Neural Syst. Rehabil. Eng., **12**(1), pp. 122–130.
[33] Grood, E. S., and Suntay, W. J., 1983, "A Joint Coordinate System for the Clinical Description of Three-Dimensional Motions: Application to the Knee," ASME J. Biomech. Eng., **105**(2), pp. 136–144.
[34] Wu, G., Siegler, S., Allard, P., Kirtley, C., Leardini, A., Rosenbaum, D., Whittle, M., D′Lima, D. D., Cristofolini, L., and Witte, H., 2002, "ISB Recommendation on Definitions of Joint Coordinate System of Various Joints for the Reporting of Human Joint Motion-Part I: Ankle, Hip, and Spine," J. Biomech., **35**(4), pp. 543–548.
[35] Perry, J., 1992, *Gait Analysis: Normal and Pathological Function*, Slack, Thorofare, NJ.
[36] USNRC Technical Training Center, 2003, "Dose Standards and Methods for Protection Against Radiation and Contamination," Rev. 0603, U.S. Nuclear Regulatory Commission, Washinigton, DC, p. 8-3.